

Article

Study on Comprehensive Technology of Preventing Mud Cake of Large Diameter Slurry Shield in Composite Stratum

Yuan Mei ^{1,2}, Dongbo Zhou ^{1,2,*}, Hang Gong ^{1,2}, Xin Ke ^{1,2}, Wangyang Xu ^{1,2} and Wenyan Shi ^{1,2}¹ School of Civil Engineering, Xi'an University of Architecture & Technology, Xi'an 710055, China² Shaanxi Key Lab of Geotechnical and Underground Space Engineering, Xi'an 710055, China

* Correspondence: zdb@xauat.edu.cn

Abstract: When large-diameter slurry shields are tunneling in a composite stratum with a high clay content, the cutter head may form a mud cake. After the mud cake is formed, it will cover the cutter and reduce the opening rate of the cutter head, thus reducing the penetration of the cutter and the driving speed. Based on a road upgrading project, this paper studies the prevention and treatment of a mud cake and forms a set of comprehensive treatment methods. For a large mud cake, through theoretical analysis, two calculation methods of the cutter head sealing coefficient are obtained, and the cutter head sealing coefficient relationship model is established. Comparing the calculated cutter head's actual opening coefficient with the required cutter head opening coefficient can provide a judgment basis for the time of manual warehousing. For medium and small mud cakes, the numerical simulation is carried out based on the cutter head and the scouring system, the distribution characteristics of the flow field near the cutter head are analyzed, and the angle of the central scouring hole is optimized. For a small mud cake, hydrogen peroxide is selected as an additive through microscopic mechanism analysis. The effect of the hydrogen peroxide solution concentration on dissolving a mud cake is obtained through laboratory tests, and its effectiveness is verified through field tests. The research results can provide a reference for the mud cake prevention of slurry shields in similar strata.

Keywords: slurry shield; mud cake; cutter head sealing coefficient; numerical simulation; scour system; hydrogen peroxide solution



Citation: Mei, Y.; Zhou, D.; Gong, H.; Ke, X.; Xu, W.; Shi, W. Study on Comprehensive Technology of Preventing Mud Cake of Large Diameter Slurry Shield in Composite Stratum. *Buildings* **2022**, *12*, 1555. <https://doi.org/10.3390/buildings12101555>

Academic Editor: Abdelhafid Khelidj

Received: 4 September 2022

Accepted: 22 September 2022

Published: 28 September 2022

Publisher's Note: MDPI stays neutral with regard to jurisdictional claims in published maps and institutional affiliations.



Copyright: © 2022 by the authors. Licensee MDPI, Basel, Switzerland. This article is an open access article distributed under the terms and conditions of the Creative Commons Attribution (CC BY) license (<https://creativecommons.org/licenses/by/4.0/>).

1. Introduction

With the continuous development of urbanization in China, the contradiction between the limited land resources and the increasing urban population is becoming increasingly serious [1–3]. To relieve the urban traffic pressure, the comprehensive utilization of urban underground space resources has become an inevitable trend of urban development [4–7]. The shield method has become a common way to construct various tunnels because it can be applied in various strata and has advantages such as high construction safety guarantee, small impact on surrounding areas and fast construction speed [8–10]. However, when the shield machine is driven in the soil layer with a high clay content, it is very easy to encounter the engineering technical problem, that is the cutter head forming a mud cake [11–13]. Mud cake refers to the semi consolidated or consolidated soil mass formed by the accumulation of small soil blocks and debris under the rotary cutting of the cutter head at or near the cutter head opening. Once the cutter head forms mud cake, it will not only reduce the driving speed, affect the tunnel forming quality, but also threaten construction safety [14–17]. In order to reduce the influence of cutter head mud cake on shield parameters, researchers studied the adsorption performance of cutter head metal materials, the thermal damage law of cutter head mud cake, and the dispersion performance of mud cake regulator on mud cake from the perspective of the model test, field test, and numerical simulation.

There are various kinds of metals used in the shield cutter head, and the adsorption of different metals on the soil is different. Qiu found through the model test that the soil has good adhesion to aluminum and poor adsorption to steel and copper, which has a guiding role in the selection of cutter head manufacturing materials [18]. Hyobum Lee and Gong [19,20] have developed a variety of shield cutter head monitoring systems, which can view the status of mud cake on the cutter head in real time and formulate corresponding measures to prevent mud cake. Through numerical simulation, theoretical analysis, and experimental research, Gong, Yang, Ulku Kalayci Sahinoglu [20,21] explained the role of mud cake on shield tunneling parameters and found that the existence of mud cake increased the friction between soil and cutter head, and the temperature of cutter head continued to rise during shield tunneling, accelerating the thermal damage of cutter head [22,23]. At the same time, Hu [24] found that the mud cake will increase the torque of the cutter head during tunneling, accelerate the energy consumption during shield tunneling, and reduce construction efficiency. G Meschke considers the process of mud cake formation on the excavation face during shield tunneling and shutdown, which can better predict and control the mud cake formation at various stages of shield construction [25].

In order to reduce the influence of mud cake on shield tunneling parameters, Christoph Budach, Kim and Daniele Peila [26–28] developed a variety of soil conditioners to decompose mud cake on the cutter head. However, due to the complexity and dispersion of the physical and mechanical properties of soil, it is difficult to have a general soil conditioner applicable to various strata. Although with the development of material science and the progress of analysis methods, the mechanism of soil conditioners is more clear, and the application scope is constantly expanding. However, with the expansion of the scope of shield engineering practice, the current research on soil conditioners still needs to be continued to increase the ability of decomposing mud cake [14,29,30]. At the same time, the cutter head scouring system uses high-pressure water to wash the soil attached to the cutter head, reducing the possibility of sludge cake on the cutter head. Since then, the scouring system has continued to develop. Xiao [31] has continuously improved and innovated the structural form and scouring angle of the cutter head scouring system, further reducing the probability of sludge cake formation on the cutter head.

The above studies have little research on the mud cake of the cutter head of the large-diameter slurry shield, and less research on the complete set of mud cake prevention measures for the optimization of the cutter head scouring system and the mud cake dissolving solution. Based on this, this paper relies on a large-diameter slurry shield project to analyze the risk of mud cake formation on the cutter head from theoretical analysis, numerical simulation, and indoor and outdoor tests. The scour angle of the cutter head scour system and the proportion of mud cake solution was studied. The research results of this paper are expected to provide a reference for similar projects and provide a design and theoretical basis for the prevention and control of sludge cake on the cutter head.

2. Project Overview of Test Section

An air cushion mud water balance shield machine with a diameter of 13.46 m is used in a road upgrading and reconstruction project. The cutter head structure adopts a composite layout of panels and spokes, with an overall opening rate of about 31%. The cutter head structure is shown in Figure 1a.

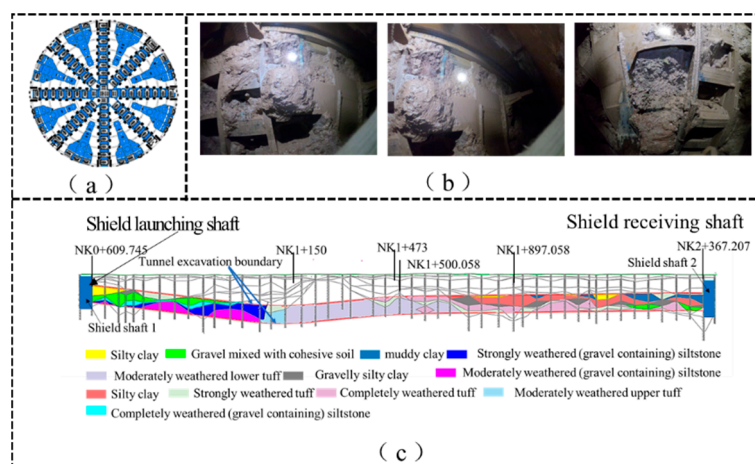


Figure 1. Project overview of test section; (a) schematic diagram of shield cutter head structure; (b) mud cake forming the state of cutter head; (c) soil layer distribution in shield tunneling area.

There are soft upper and hard lower composite strata in the shield tunneling area. The main soil layers are silty clay, gravel mixed with cohesive soil, moderately weathered tuff, fully weathered tuff, etc., of which clay accounts for more than 50%. The distribution of soil layers in the shield tunneling area is shown in Figure 1c. It is very easy to produce mud cake during tunneling in this section. The appearance of mud cake will not only lead to the deterioration of shield parameters but also delay the construction progress and even threaten the construction safety. The mud cake in the mud tank is shown in Figure 1b. It can be seen from the Figure that there is a serious mud cake phenomenon on the site.

3. Active Opening and Clearing

Before the large mud cake is formed, industrial lubricants such as washing powder, bleach powder, and detergent are added to the mud. The shield washing system uses the slurry or water flow with a certain pressure to wash and separate the crushed soil blocks and debris adhered around the cutter head. The centrifugal force generated by the idling of the cutter head at a high speed will separate the soil blocks from the cutter head surface or make the mud cake difficult to form. However, when the sludge cake is generated rapidly, the idling and scouring methods are ineffective or the effect is poor, the residual soil in the soil tank will continue to accumulate and gradually fill the gaps between the spokes of the cutter head and the panel, and between the cutter and the cutter box, and finally fill the whole mud tank. In this case, the mud cake can only be cleaned manually by workers entering the soil tank.

3.1. Analysis of Shield Tunneling Parameters after Manual Mud Cake Removal

After the 132, 138, and 145 ring segments are installed, it takes 2, 3, and 8 days to manually clean the mud cake of the cutter head. Statistics show that the total amount of mud cake removed increases with the increase of segment ring number. At the same time, the corresponding shield tunneling parameters in this stage are statistically analyzed, and the results are shown in Figure 2. It can be seen from Figure 2 that after the mud cake is manually removed, the shield tunneling speed and the penetration of the shield cutter head increase. However, after the mud cake is removed from ring 132, the thrust of the shield and the torque of the shield cutter head still have an upward trend; In contrast, after all mud cakes are removed in ring 145, the shield tunneling speed, cutter penetration, total thrust of shield and cutter head torque have been significantly improved. Therefore, it can be determined that the improvement effect of the above parameters is positively related to the mud cake removal amount. In ring 132, the effect is not obvious because the mud cake is not completely cleaned.

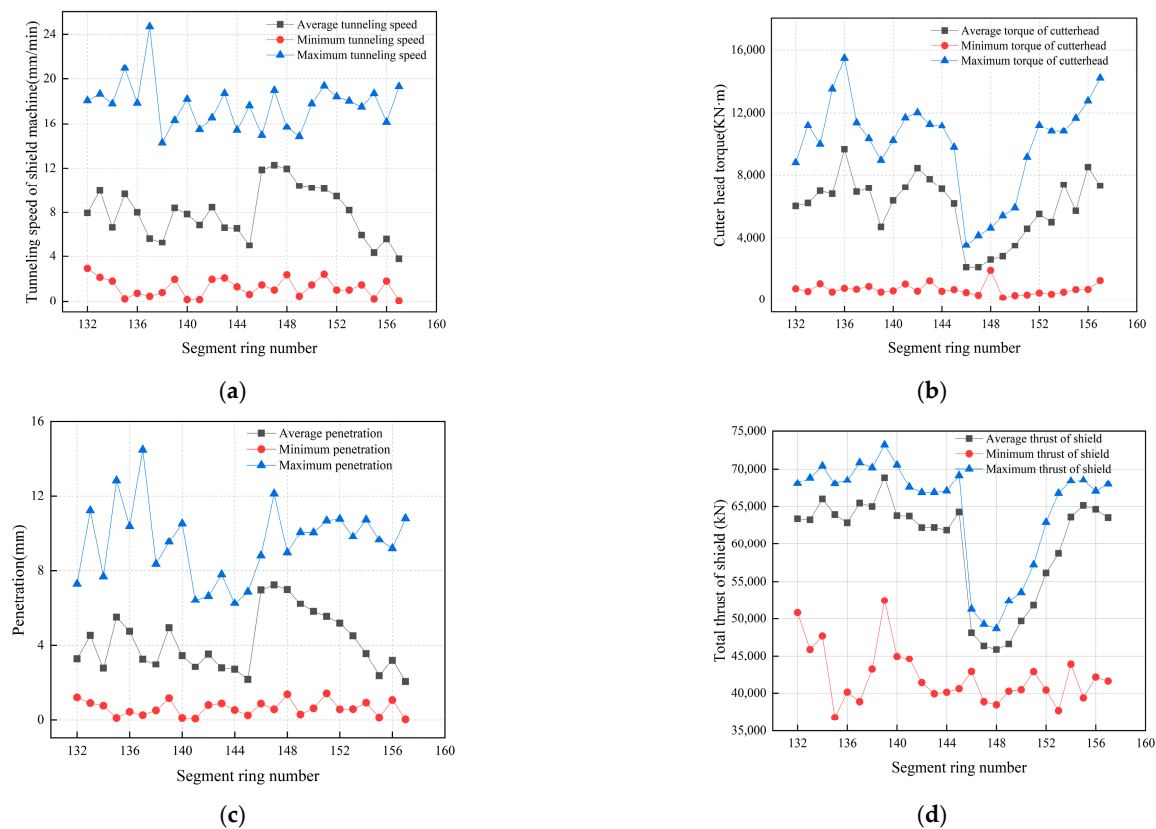


Figure 2. Influence of mud cake cleaning on shield parameters; (a) influence of mud cake cleaning on driving speed; (b) influence of mud cake cleaning on penetration; (c) Influence of mud cake cleaning on the total thrust of the shield; (d) effect of mud cake cleaning on cutter head torque.

Due to the correlation between mud cake cleaning amount and time, after considering the time factor, the relationship among shield parameters, mud cake cleaning amount, and time factor can be further modified as follows: less mud cake cleaning amount, less time consumption, and no obvious change in shield parameters. The amount of mud cake cleaning is large, the consumption time is large, and the shield parameters change obviously. The optimal state of shield parameters is to clear all the mud cake, but with the accumulation of mud cake, the difficulty of mud cake cleaning increases, the cleaning speed decreases, and the time required increases; If the mud cake is cleaned frequently, the construction process will increase, and the time cost will also increase. Therefore, arranging the personnel to enter the cabin for cleaning is a problem that needs to be clarified for manual cleaning of mud cake.

3.2. Calculation of Cutter Head Sealing Coefficient

The cumulative amount of mud cake of the cutter head can be reflected by the actual opening rate of the cutter head, and the actual opening rate of the cutter head can be obtained by the sealing coefficient of the cutter head. When the mud cake amount is zero, the sealing coefficient of the cutter head is the design opening rate. When the mud cake is spread on the cutter head, the actual opening rate of the cutter head is zero.

The torque of the shield cutter head consists of the following nine parts [24,32,33]:

$$M = M_1 + M_2 + M_3 + M_4 + M_5 + M_6 + M_7 + M_8 + M_9 \quad (1)$$

where: M is the total torque of the shield cutter head; M_1 is the cutting torque of the tool; M_2 is the rotation moment generated by the dead weight of the cutter head; M_3 is the rotational moment generated by the thrust load of the cutter head; M_4 is the friction torque

generated by the sealing device; M_5 is the friction torque on the front surface of the cutter head; M_6 is the friction torque on the circumferential surface of the cutter head; M_7 is the friction torque on the back of the cutter head; M_8 is the shear moment of the cutter head opening groove; M_9 is the stirring torque in the soil chamber of the cutter head.

$$M_1 = \frac{1}{2} (C_1 h_{\max} R_0^2) \quad (2)$$

where: C_1 is the shear strength of soil; $C_1 = C + P_d \times \tan\varphi$; C is the cohesion of soil; P_d is the horizontal earth pressure; h_{\max} is the maximum cutting depth of the cutter head per revolution; R_0 is the radius of the outermost cutter.

$$M_2 = GRu_g \quad (3)$$

where: G is the dead weight of the cutter head; R is the contact radius of the bearing; u_g is the rolling friction coefficient.

$$M_3 = W_p R_g u_g \quad (4)$$

where: W_p is thrust load; $W_p = \alpha \pi R_c^2 P_d$; α is the sealing coefficient of cutter head; R_c is the radius of cutter head; R_g is the contact radius of bearing thrust roller.

$$M_4 = 2\pi u_m F (n_1 R_{m1}^2 + n_2 R_{m2}^2) \quad (5)$$

where: u_m is the friction coefficient between seal and steel; F is the sealing thrust; n_1, n_2 is the number of seals; R_{m1}, R_{m2} , is the installation radius of the seal.

$$M_5 = \frac{2}{3} (\alpha \pi u_p R_c^3 P_d) \quad (6)$$

where: u_p is the friction coefficient between the soil layer and the cutter head.

$$M_6 = 2\pi R_c^2 B P_Z u_p \quad (7)$$

where: B is the cutter head width; P_Z is the earth pressure around the cutter head.

$$M_7 = \frac{2}{3} [(1 - \alpha) \pi R_c^3 u_p \times 0.8 P_d] \quad (8)$$

$$M_8 = \frac{2}{3} \pi C_1 R_c^3 \alpha \quad (9)$$

$$M_9 = 2\pi (d_1^2 - d_2^2) L C_1 \quad (10)$$

where: d_1 is the outer diameter of cutter head support beam; d_2 is the inner diameter of cutter head support beam; L is the length of the support beam.

In order to get the actual situation of the cutter head opening rate at any time, two methods for calculating the cutter head sealing coefficient are provided.

Method 1: Equation (11) is obtained by modifying Equation (1).

$$M_3 + M_5 + M_7 + M_8 = M - M_1 - M_2 - M_4 - M_6 - M_9 \quad (11)$$

Substituting Equations (4), (6) and (8) into Equation (9) to obtain Equation (12):

$$\alpha = \frac{M - M_1 - M_2 - M_4 - M_6 - M_9}{\pi R_c^3 \left(\frac{R_g}{R_c} P_d u_g + \frac{2}{15} P_d u_p + \frac{2}{3} C_1 \right)} \quad (12)$$

Simultaneous Equations (2), (3), (5), (7) and (10) can further obtain the actual opening of the cutter head.

Method 2: Set the cutter head torque at t_2 as:

$$M = M'_1 + M'_2 + M'_3 + M'_4 + M'_5 + M'_6 + M'_7 + M'_8 + M'_9 \quad (13)$$

Subtract the cutter head torque at t_2 from the initial cutter head torque at t_1 :

$$\begin{aligned} & M'_3 - M_3 + M'_5 - M_5 + M'_7 - M_7 + M'_8 - M_8 \\ &= (M' - M) - (M'_1 - M_1) - (M'_2 - M_2) - (M'_4 - M_4) - (M'_6 - M_6) - (M'_9 - M_9) \end{aligned} \quad (14)$$

Similarly, subtracting M'_3 and M_3 , M'_5 and M_5 , M'_7 and M_7 , M'_8 and M_8 is deformed as follows:

$$M'_3 - M_3 = R_g u_z \pi R_c' (P'_d \alpha' - P_d \alpha) \quad (15)$$

$$M'_5 - M_5 = \frac{2}{3} u_p \pi R_c^3 (P'_d \alpha' - P_d \alpha) \quad (16)$$

$$M'_7 - M_7 = \frac{8}{15} \pi u_p R_c^3 [P'_d (1 - \alpha') - P_d (1 - \alpha)] \quad (17)$$

$$M'_8 - M_8 = \frac{2}{3} \pi R_c^3 (C'_1 \alpha' - C_1 \alpha) \quad (18)$$

Formula (19) is obtained by substituting Formulas (15)–(18) into formula (14):

$$\alpha' = \frac{(M' - M) - (M'_1 - M_1) - (M'_2 - M_2) - (M'_4 - M_4) - (M'_6 - M_6) - (M'_9 - M_9)}{\pi R_c^3 (\frac{2}{3} C'_1 + \frac{R_g}{R_c} u_z P'_d + \frac{7}{15} u_p P'_d)} \quad (19)$$

Since the rotating moment M_2 generated by the dead weight of the cutter head, the friction moment M_4 generated by the sealing device, and the stirring moment M_9 in the soil chamber of the cutter head are determined by the shield itself and remain basically unchanged at any time, the Formula (19) can be further simplified as:

$$\alpha' = \frac{(M' - M) - (M'_1 - M_1) - (M'_6 - M_6)}{\pi R_c^3 (\frac{2}{3} C'_1 + \frac{R_g}{R_c} u_z P'_d + \frac{7}{15} u_p P'_d)} \quad (20)$$

Simultaneous equations:

$$\begin{cases} \alpha' = \frac{(M' - M) - (M'_1 - M_1) - (M'_6 - M_6)}{\pi R_c^3 (\frac{2}{3} C'_1 + \frac{R_g}{R_c} u_z P'_d + \frac{7}{15} u_p P'_d)} \\ M'_1 - M_1 = \frac{1}{2} R_0^2 h_{\max} (C'_1 - C_1) \\ M'_6 - M_6 = 2 \pi R_c^2 B u_p (P'_z - P_z) \end{cases} \quad (21)$$

The actual sealing coefficient of the cutter head at T2 can be obtained by the rescue equation group (21).

3.3. Model Establishment

The relevant data of three consecutive manual cleaning of mud cake are listed above. When other conditions remain unchanged after the first mud cake cleaning is completed, the shield machine shall continuously drive 6 rings of segments. After the second mud cake cleaning is completed, the shield machine shall continuously drive the distance of seven ring segments. After the third mud cake cleaning is completed, the shield machine shall continuously drive 12 ring segments. Since there are only two variables, the relationship between the total amount of mud cake cleaning in a single time and the number of continuous driving rings of the shield after cleaning can be fitted by regression analysis. At the same time, with the increase of the mud cake amount of the cutter head, the mud cake thickness and the actual sealing coefficient of the cutter head will increase, and the compactness of the mud cake will also increase under the pressure, and the force required for the mud cake peeling will also increase. Assuming that each worker has a certain physical strength every day, the daily cleaning speed of mud cake will decrease. Since there are only two variables,

the relationship between the actual sealing coefficient of the cutter head and the mud cake cleaning speed per day can be fitted by regression analysis.

Considering the difference between the total amount of mud cake in the mud tank and the cutter head during the actual construction, under the condition that the cleaning amount is the same, the different ratio of the cleaning amount and the total amount of mud cake will also have an impact on the optimization effect of the shield parameters. For the convenience of analysis, the total amount of mud cake cleaning in a single time is replaced by the volume of remaining mud cake in the tank. The relationship between the volume of residual mud cake in the tank and the cleaning speed of mud cake in a single day is: $(1 - \text{volume of residual mud cake in the tank}) / \text{single cleaning time} = \text{cleaning speed of mud cake in a single day}$.

According to the above analysis, the relationship model diagram of the actual sealing coefficient of the cutter head, the cleaning speed of the mud cake in a single day, the volume of the remaining mud cake in the cabin, the number of continuous driving rings, and the single cleaning time is established, as shown in Figure 3. It can be seen from Figure 3 that by setting the number of continuous driving rings as an independent variable, the volume of residual mud cake in the cabin can be obtained, and then the cutter head sealing coefficient can be calculated by using the fitted function, and then the actual opening coefficient of the cutter head calculated can be compared with the fitted opening coefficient of the cutter head. Thus, it can provide a judgment basis for the time of entering the mud bin manually.

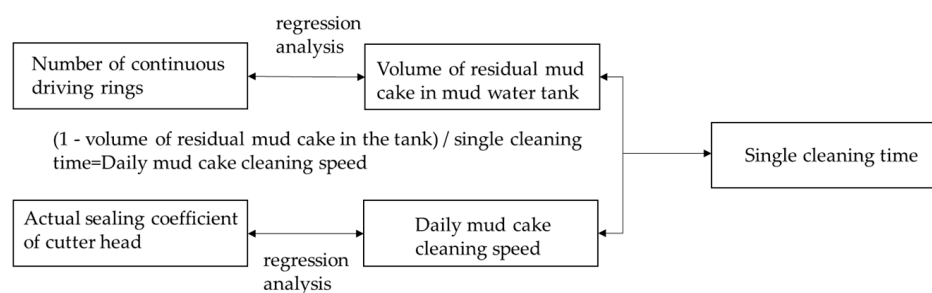


Figure 3. Regression analysis model.

4. Study on Optimal Design of Scouring Angle of Shield Central Scouring Hole

4.1. Establishment of Numerical Analysis Model

The fluid numerical simulation software is used to analyze the shield cutter head and scouring system. The established geometric model is shown in Figure 4a. There are three central scouring holes, two mud inlets, and one mud gate outlet arranged on the cutter head diaphragm. The surface of the working face is marked as an A, the front panel of the cutter head is marked as B, the rear panel of the cutter head is marked as C, and the bulkhead of the mud bin is marked as D. The mesh model is composed of three parts: stationary region I (CD inter surface region), rotating region (BC inter surface region) and stationary region II (AB inter surface region), as shown in Figure 4b.

The numerical analysis assumes that the mud is an ideal uniform fluid and the mud water density is 1136 kg/M^3 ; The dynamic viscosity of mud water is $3.184 \cdot 10^{-3} \text{ Pa}\cdot\text{s}$. In the process of shield excavation, the permeability of fluid on the face is not considered, and RNG K- ϵ equation model is selected for numerical model analysis. The combination of mass flow inlet and static pressure outlet is selected as the boundary condition.

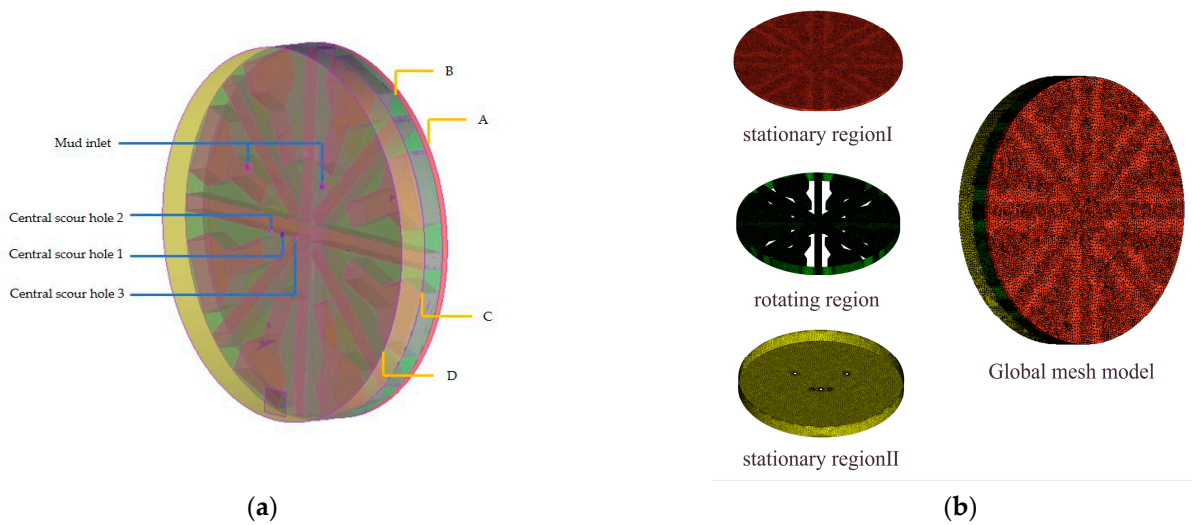


Figure 4. Numerical analysis model; (a) geometric model of cutter head; (b) cutter head mesh model.

4.2. Working Condition Design

Under the condition that the flow of the shield scour hole is kept constant, the scour angle of the center scour holes on both sides of the cutter head diaphragm center is optimized. The working condition design is shown in Table 1. Working condition 1 is the design working condition of the original scouring system while working conditions 2, 3, and 4 correspond to working conditions with scouring angles of 45°, 70°, and 90°, respectively.

Table 1. Working condition design.

Working Condition	1	2	3	4
Scour angle (°)	20	45	70	90
Flow of scouring holes 2 and 3 (m ³ /h)	300	300	300	300
Flow of scouring holes 1 (m ³ /h)	1200	1200	1200	1200
Mud inlet flow (m ³ /h)	200	200	200	200
Outlet pressure (bar)	3.3	3.3	3.3	3.3

For the convenience of description and analysis, the range of 0.00 m~2.50 M of the shield front cavity is defined as the central area, and the range of 2.50~6.73 m is defined as the outer area, as shown in Figure 5a. Since the mud cake is mainly concentrated near the cutter head, the section I is set as the section 0.01 M away from the rear panel of the cutter head, as shown in Figure 5b.

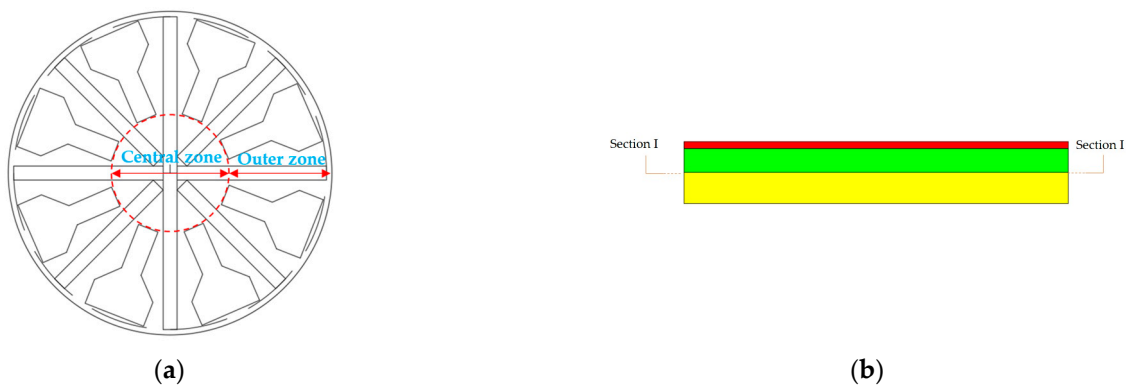


Figure 5. Model area setting; (a) division of shield front cavity area; (b) schematic diagram of a section of shield front cavity.

4.3. Result Analysis

The mud flow velocity cloud diagram and vector diagram of section I under different scouring angles are shown in Figure 6.

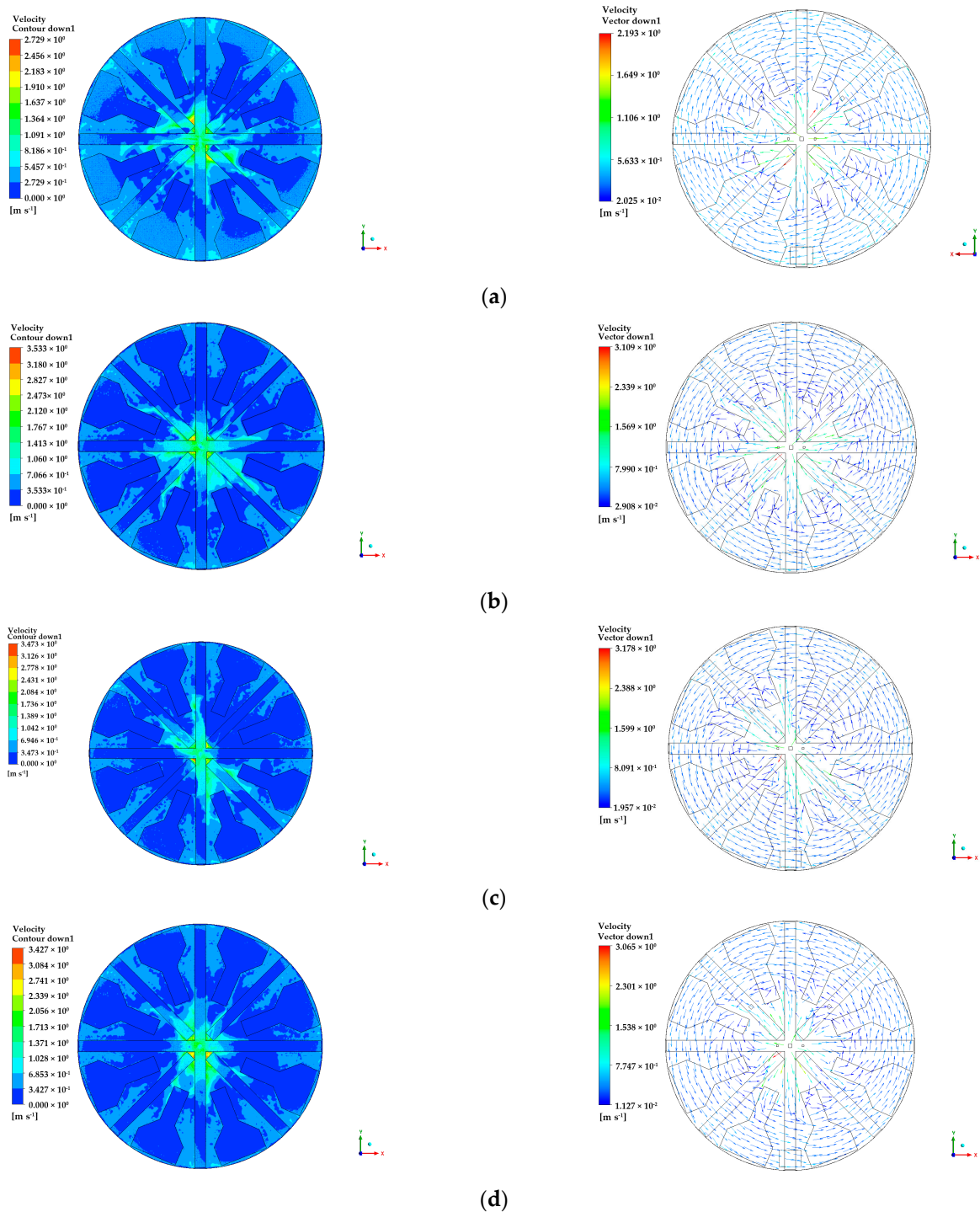


Figure 6. Cloud diagram and vector diagram of mudflow velocity of section I under different scouring angles; (a) the scouring angle is 20°; (b) the scouring angle is 45°; (c) The scouring angle is 70°; (d) the scouring angle is 90°.

According to the flow velocity cloud diagram in Figure 6a, the maximum mud flow velocities corresponding to working conditions 1, 2, 3, and 4 are 2.729 m/s, 3.533 m/s, 3.473 m/s, and 3.427 m/s, respectively, that is, when the scouring angle of central scouring holes 2 and 3 is 45° , the mud flow velocity is the maximum. From the flow velocity vector diagram in Figure 6b, it can be seen that the scouring area of the central scouring hole on the central area under the four working conditions is different, and the order from large to small is: working condition 2 > working condition 1 > working condition 4 > working condition 3. According to the above analysis, it can be determined that the optimal scouring angle of central scouring holes 2 and 3 is 45° .

Since the scouring effect of the central scouring hole on the central area is different in all directions, the above analysis only considers the maximum flow velocity and scouring range of the fluid in the flow field. In order to more comprehensively reflect the mud movement state in the central area of the section, the method shown in Figure 7 is adopted for analysis: (1) radial type: select the flow velocity value in each direction to study the law of mudflow velocity in different directions with the center distance of the cutter head; (2) Concentric circle type: select the flow velocity value on the circumference with different distance, and study the change law of the average mud flow velocity at the same distance from the cutter head center with the cutter head center distance.

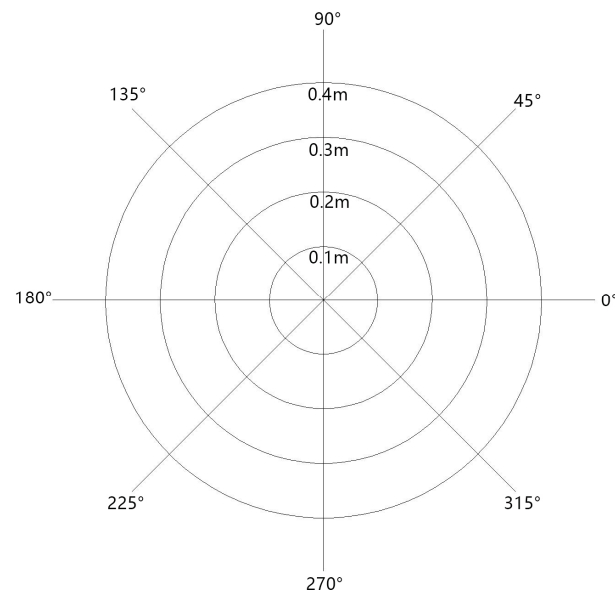


Figure 7. Schematic diagram of analysis method.

The variation law of mud flow rate in different directions under four working conditions obtained by radial method is shown in Figure 8. It can be seen from Figure 8 that the mud flow velocity in all directions increases first and then decreases, and the mud flow velocity reaches the maximum within the range of 0.5~0.7 m from the section center. The mud flow velocity in the three directions of 135° , 225° , and 315° is larger, which indicates that the scouring effect in these directions is better. However, the mud flow velocity in the direction of 90° and 270° fluctuates within the range of 0.9~2.1 m from the section center, indicating that the mud flow velocity in these two directions is not stable. The working conditions are sorted according to the maximum mud flow velocity: working condition 3 > working condition 2 > working condition 4 > working condition 1.

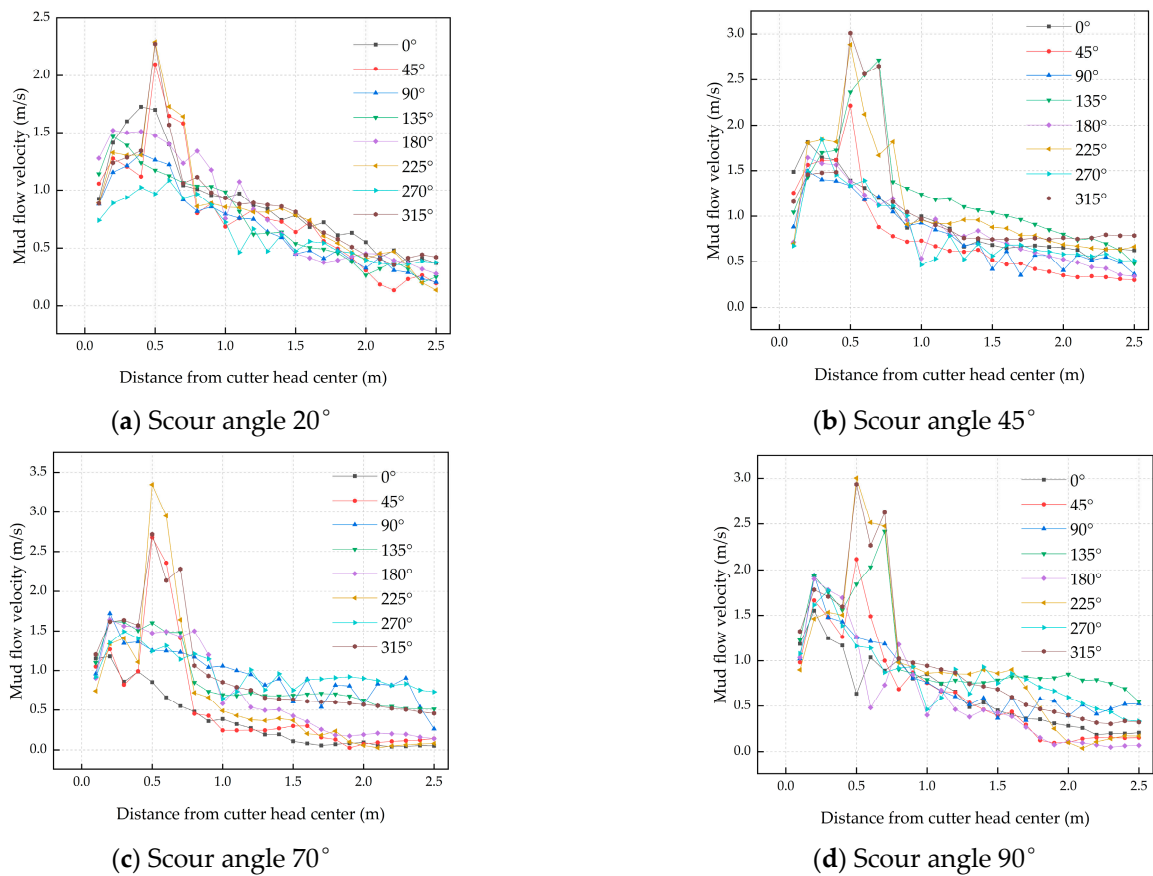


Figure 8. Curve of mud flow rate change by radial method.

The change curve of average flow velocity of mud in all directions with scouring angle under four working conditions is shown in Figure 9. It can be seen from Figure 9 that when the scouring angle of scouring holes on both sides is 45°, the average flow velocity of mud in the four directions of 135°, 180°, 225°, and 315° is higher than that of the other three schemes, and the average flow velocity of mud in other directions is also higher, which indicates that the overall scouring effect is better.

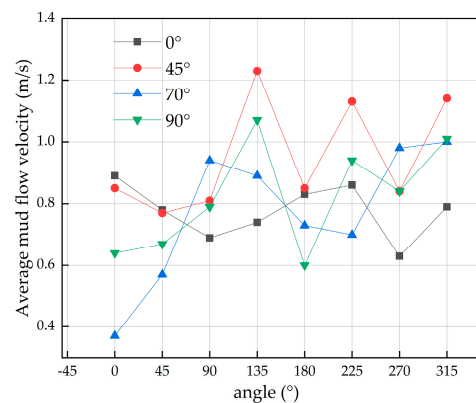


Figure 9. Variation curve of the average flow velocity of mud in each direction with scouring angle.

It can be seen from Figures 8 and 9 that when the scouring angle of the central scouring holes on both sides is 45°, the maximum mud flow velocity is 3.01 m/s, which is only lower than 3.35 m/s of working condition 3, higher than 2.29 m/s of working condition 1 and 3.00 m/s of working condition 4. According to the maximum mud flow velocity and the average mud flow velocity in each direction of section I, when the scouring angle

of the central scouring holes on both sides is set to 45° , the internal area will be scoured more fully.

The concentric circle method is used to study the variation of the average flow velocity of mud with the distance from the center of the section. The variation curve of the average flow velocity of mud with the distance in the center area of section I is shown in Figure 10. It can be seen from Figure 10 that the average flow velocity of mud under the four working conditions increases first and then decreases with the increase of distance. The maximum average flow velocity of mud under each working condition occurs at 0.5 m from the center of the section. The maximum average flow velocity of mud under working conditions 1, 2, 3, and 4 is 1.65 m/s, 1.99 m/s, 1.90 m/s, and 1.78 m/s, respectively. The average flow velocity of mud under working condition 2 is the maximum.

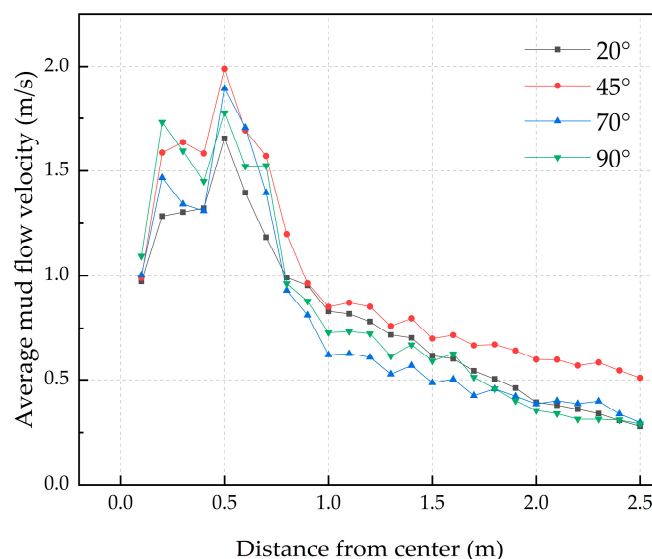


Figure 10. Variation curve of the average flow velocity of equidistant mud with distance.

According to the comparative analysis, when the scouring angle is 20° , the average flow velocity of mud is the smallest within the range of 0.1~0.7 m from the section center. When the scouring angle is 45° , the average flow velocity of mud at the range of 0.3~0.5 m and 0.7~2.5 m from the section center is greater than the corresponding value of other working conditions; When the scouring angle is 70° , the average flow velocity of the mud is the smallest in the range of 0.8~1.7 m; When the scouring angle is 90° , the average flow velocity of mud is the smallest within the range of 1.8~2.4 m. According to the average flow velocity of mud at equal distances from the inner area of section I to the center of the section, it can be judged that when the scouring angle of the central scouring holes on both sides is set to 45° , it is more conducive to scouring the inner area of the cutter head.

According to the above comprehensive judgment of the maximum mud flow velocity of section I, the area of the central scouring area, the maximum mud flow velocity and the average mud flow velocity in all directions of the central area of section I, and the average mud flow velocity at equal distances from the central area of section I to the center of the section, the scouring effect is the best when the scouring angle of the central scouring holes on both sides is set to 45° .

5. Chemical Cleaning of Cutter Head Mud Cake

5.1. Composition Analysis of Mud Cake

XRD is the abbreviation of “X-ray diffraction”. It uses X-ray to diffract materials and then analyzes the diffraction pattern to obtain the material composition, internal atomic composition, and chemical structure of elements. It is an important material science research technology.

Collect the soil attached to the cutter head of the north and south lines of the shield, and conduct mineral composition analysis with a D8 advance X-ray diffractometer, as shown in Tables 2 and 3. The sampling analysis process is shown in Figure 11.

Table 2. Mineral composition of mud cake on the north line.

Component	Chemical Formula	Mass Percentage/%
Calcium montmorillonite	$\text{Ca}_{0.2}(\text{Al,Mg})_2\text{Si}_4\text{O}_{10}(\text{OH})_2$	59.8
Illite (hydromica)	$(\text{KH}_3\text{O})\text{Al}_2\text{Si}_3\text{AlO}_{10}(\text{OH})_2$	2.1
Potash feldspar	KAlSi_3O_8	0.5
quartz	SiO_2	37.6

Table 3. Mineral composition of mud cake on the south line.

Component	Chemical Formula	Mass Percentage/%
Calcium montmorillonite	$\text{Ca}_{0.2}(\text{Al,Mg})_2\text{Si}_4\text{O}_{10}(\text{OH})_2$	33.4
Illite (hydromica)	$(\text{KH}_3\text{O})\text{Al}_2\text{Si}_3\text{AlO}_{10}(\text{OH})_2$	12.8
Calcium feldspar	$\text{Ca}(\text{Al}_2\text{Si}_2\text{O}_8)$	4.0
calcite	CaCO_3	9.9
quartz	SiO_2	39.9



Figure 11. Composition analysis of mud cake; (a) X-ray diffractometer; (b) soil sample of north line; (c) soil sample of south line.

It can be seen from the table that in the mineral composition of mud cake in the north line, calcium montmorillonite and illite, which belong to clay minerals, account for 61.9% of the total sample mass; In the mineral composition of mud cake in the south line, calcium montmorillonite and illite, which belong to clay minerals, account for 46.2% of the total sample mass.

5.2. Selection of Admixture

The soil viscosity is mainly due to the negative charge of clay mineral particles in the water, which forms an electric field around the soil particles, attracts cations and water molecules in the water, and forms a common water film. Finally, the tension of water causes cohesion between soil particles [34,35]. The practice has proved that the method of adding an oxidant to oxidize the organic matter between clay particles can enhance the hydration ability of cations [36,37], thus achieving the purpose of delaying the formation rate of mud cake. The surface electrification of clay is shown in Figure 12.

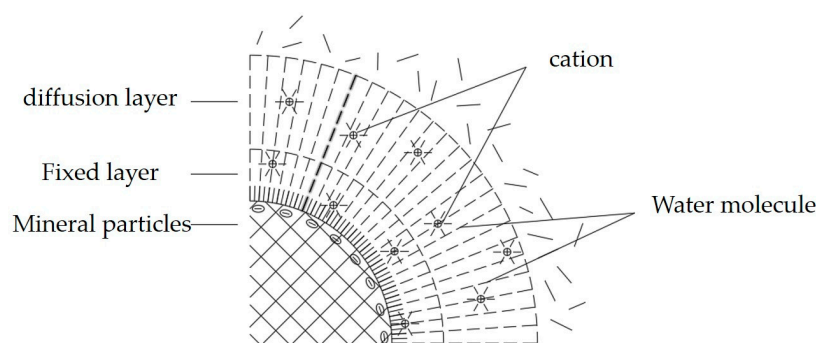


Figure 12. Surface electrification of clay.

Hydrogen peroxide (H_2O_2) is a strong oxidant. In addition, hydrogen peroxide can increase the layer spacing of Muscovite crystal from 0.912 nm to 0.999 nm, which can cause chemical expansion of Muscovite, making it easier to exfoliate and dissolve in solution. Moreover, its chemical reaction products are mainly water (H_2O) and oxygen (O_2), which have no pollution to the environment. Therefore, hydrogen peroxide is selected as the chemical agent to peel the clay. The specific test steps are as follows:

- (1) Remove the mud cake material from the cutter head and evenly divide it into 4 clay samples;
- (2) Mix 35% hydrogen peroxide solution with the mud of different quality to prepare different concentration solutions required for the test;
- (3) Put the clay block into the solution and record the change of the mass of the clay block with time.

When the clay block is immersed in the hydrogen peroxide solution, bubbles are constantly generated in the solution. In addition, the measured temperature of the solution rises. After the test is completed, the variation of the measured clay mass with the solution concentration is shown in Table 4.

Table 4. Variation of clay mass with solution concentration.

Time (min)	Mass of Clay Block (g, 5%)			
0	665.38	665.98	652.01	665.34
15	502.12	595.87	601.13	621.46
25	415.64	480.32	569.55	589.85
35	386.94	424.35	531.26	565.54
45	370.41	395.50	500.32	560.25
55	359.82	386.05	462.43	546.27
65	356.74	379.02	459.12	541.44
185	348.59	374.88	441.75	521.60

It can be seen from Table 4 that when the reaction time reaches 50–60 min, although the mass of the clay block continues to decrease, the decrease slows down. Therefore, it is judged that the effective reaction time of the solution is approximately 1 h. Further calculation shows that the mass of the clay block is reduced by 47.6%, 43.7%, 32.25%, and 21.6% respectively in the solution with the concentration of 5%, 4%, 3%, and 2%. The reduction of the mass of the clay block is basically proportional to the concentration of the hydrogen peroxide solution. Through a horizontal comparison of the four test results, it can be seen that when the concentration of hydrogen peroxide solution is 4% and 5%, the dissolution effect of clay is better. However, compared with the 4% concentration of hydrogen peroxide solution, the 5% concentration of hydrogen peroxide solution can not significantly increase the weight of the dissolved clay block. Considering the engineering economy, the 4% concentration of hydrogen peroxide solution is selected for field use.

5.3. Effect Analysis of Engineering Practice

4% hydrogen peroxide solution is used to soak the mud bin. The penetration monitoring data obtained before and after soaking the mud bin are shown in Figure 13.

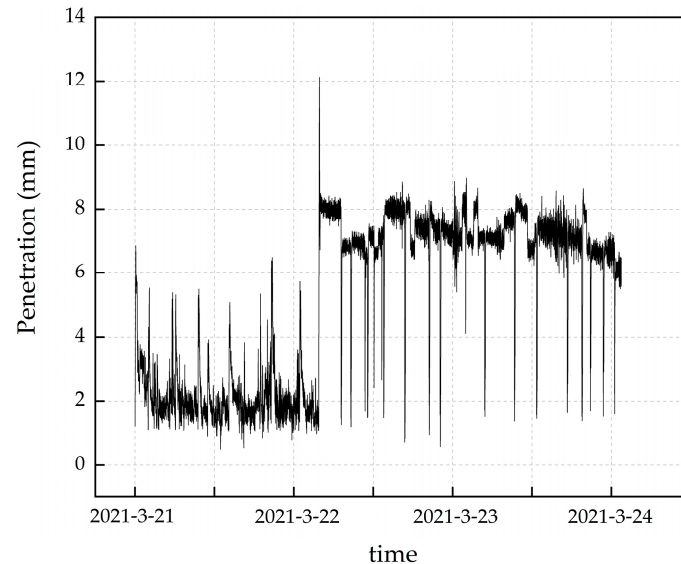


Figure 13. Effect of hydrogen peroxide solution on penetration.

The hydrogen peroxide field soaking was carried out from 22 March 2021 to 23 March 2021. It can be seen from Figure 13 that after soaking the bin body with a hydrogen peroxide solution, the penetration of the cutter head has been significantly improved. The average value of the single-day penetration is 7.25 mm and 7.03 mm respectively two days after soaking the bin body, which is far greater than the 2.14 mm before soaking the bin body. Since penetration = tunneling speed/rotation speed, and tunneling speed is related to thrust, the thrust will change differently when the shield machine is started and stopped, so it will have different effects on penetration, which leads to “peak” and “valley” of monitoring data. It should be noted that the hydrogen peroxide solution will generate gas during the process of soaking the mud cake. In order to prevent the gas from damaging the stability of the face and inducing surface subsidence, the overflowing gas must be discharged by the jet fan in time and the time of soaking the bin with hydrogen peroxide must be strictly controlled.

6. Conclusions

Based on the background of a road upgrading project, the anti mud cake technology of large-diameter slurry shield in composite formation is studied through numerical simulation, indoor and field tests, and theoretical derivation. The following conclusions are obtained:

- (1) Through theoretical analysis, two calculation methods of cutter head sealing coefficient are obtained. The mathematical models of the actual sealing coefficient of the cutter head, the cleaning speed of the mud cake in a single day, the volume of the remaining mud cake in the cabin, the number of continuous driving rings, and the cleaning time of a single time are established. The calculated actual opening coefficient of the cutter head is compared with the required opening coefficient of the cutter head, which can provide a judgment basis for the time of manual warehousing.
- (2) When the scouring angle of the central scouring holes on both sides of the cutter head is set to 45°, the scouring range of the mud hole and the mud flow speed are the fastest; The radial method analysis shows that the average flow velocity of mud in all directions is high under 45° working condition. According to the analysis of the concentric circle method, the average flow velocity of mud at the equidistant position

under 45° working conditions is the largest. According to comprehensive judgment, when the scouring angle of the central scouring holes on both sides is set to 45°, the scouring effect is the best.

- (3) After microanalysis, hydrogen peroxide solution is selected as the additive for mud cake decomposition. The test analysis shows that the mud cake soaked with hydrogen peroxide solution will undergo an oxidation reaction and generate bubbles. The decrease of clay mass is positively related to the solution concentration, and the increment of clay mass decrease increases first and then decreases with the increase of solution concentration.

Author Contributions: Y.M.: Conceptualization, funding acquisition, methodology, supervision, writing—review and editing. D.Z.: data curation, formal analysis, writing—original draft, validation, visualization, investigation. H.G.: resources. X.K.: resources. W.X.: resources. W.S.: resources. All authors have read and agreed to the published version of the manuscript.

Funding: The research described in this paper was financially supported by the National Natural Science Foundation of China [Grant No. 52178302], and the Key R & D Projects in Shaanxi Province [No. 2020SF-373].

Conflicts of Interest: The authors declare no conflict of interest.

References

1. Zizka, Z.; Britta, S.; Markus, T. Investigations on transient support pressure transfer at the tunnel face during slurry shield drive part 1: Case A—Cutting depth exceeds shallow slurry penetration depth. *Tunn. Undergr. Space Technol.* **2021**, *118*, 104168. [[CrossRef](#)]
2. Wang, X.; Song, Q.; Gong, H. Research on Deformation Law of Deep Foundation Pit of Station in Core Region of Saturated Soft Loess Based on Monitoring. *Adv. Civ. Eng.* **2022**, *2022*, 7848152. [[CrossRef](#)]
3. Mokhtari, S.; William, N.; Michael, M. White-box regression (elastic net) modeling of earth pressure balance shield machine advance rate. *Autom. Constr.* **2020**, *115*, 103208. [[CrossRef](#)]
4. Mei, Y.; Zhou, D.; Wang, X.; Zhao, L.; Shen, J.; Zhang, S.; Liu, Y. Deformation Law of the Diaphragm Wall during Deep Foundation Pit Construction on Lake and Sea Soft Soil in the Yangtze River Delta. *Adv. Civ. Eng.* **2021**, *2021*, 6682921. [[CrossRef](#)]
5. Yuan, B.; Li, Z.; Chen, W.; Zhao, J.; Lv, J.; Song, J.; Cao, X. Influence of Groundwater Depth on Pile–Soil Mechanical Properties and Fractal Characteristics under Cyclic Loading. *Fractal Fract.* **2022**, *6*, 198. [[CrossRef](#)]
6. Wang, X.; Ma, Z.; Zhang, Y. Research on Safety Early Warning Standard of Large-Scale Underground Utility Tunnel in Ground Fissure Active Period. *Front. Earth Sci.* **2022**, *10*, 3389. [[CrossRef](#)]
7. Santa, C.; Luís, G.; Chaminé Helder, I. A comparative study of GSI chart versions in a heterogeneous rock mass media (Marão tunnel, north Portugal): A reliable index in geotechnical surveys and rock engineering design. *Bull. Eng. Geol. Environ.* **2019**, *78*, 5889–5903. [[CrossRef](#)]
8. Do, N.A.; Dias, D.; Vu, T.T.; Dang, V.K. Impact of the shield machine’s performance parameters on the tunnel lining behaviour and settlements. *Environ. Earth Sci.* **2021**, *80*, 507. [[CrossRef](#)]
9. Jafari, P.; Ahmad, F. Upper-Bound face stability analysis of rectangular shield-driven tunnels in undrained clays. *Comput. Geotech.* **2022**, *146*, 104739. [[CrossRef](#)]
10. Wang, X.; Gong, H.; Song, Q.; Yan, X.; Luo, Z. Risk Assessment of EPB Shield Construction Based on the Nonlinear FAHP Method. *Adv. Civ. Eng.* **2022**, *2022*, 9233833. [[CrossRef](#)]
11. Huang, X.; Liu, Q.; Chen, L.; Pan, Y.; Liu, B.; Kang, Y.; Liu, X. Cutting force measurement and analyses of shell cutters on a mixshield tunnelling machine. *Tunn. Undergr. Space Technol.* **2018**, *82*, 325–345. [[CrossRef](#)]
12. Zhao, S.; Li, S.; Wan, Z.; Wang, M. Dispersant for Reducing Mud Cakes of Slurry Shield Tunnel Boring Machine in Sticky Ground. *Adv. Mater. Sci. Eng.* **2021**, *2021*, 5524489. [[CrossRef](#)]
13. Zhang, Z.; Zhang, K.; Dong, W.; Zhang, B. Study of Rock-Cutting Process by Disc Cutters in Mixed Ground based on Three-dimensional Particle Flow Model. *Rock Mech. Rock Eng.* **2020**, *53*, 3485–3506. [[CrossRef](#)]
14. Qiu, T.; Liu, C.; Zhong, X.; Zhu, Y. Experimental Research on the Impact of Temperature on the Adhesion Characteristics of Soil-Structure Interface. *Geofluids* **2020**, *2020*, 6675576. [[CrossRef](#)]
15. Gong, C.; Wang, Y.; Peng, Y.; Ding, W. Three-dimensional coupled hydromechanical analysis of localized joint leakage in segmental tunnel linings. *Tunn. Undergr. Space Technol.* **2022**, *130*, 104726. [[CrossRef](#)]
16. Lei, M.; Cui, T. A Scientometric Analysis and Visualization of Global LEED Research. *Buildings* **2022**, *12*, 1099. [[CrossRef](#)]
17. Zhou, Z.; Zhang, J.; Gong, C. Automatic detection method of tunnel lining multi-defects via an enhanced You Only Look Once network. *Comput. Aided Civ. Infrastruct. Eng.* **2022**, *37*, 762–780. [[CrossRef](#)]
18. Qiu, T.; Zhang, Y. Experimental Research on the Adhesion Characteristics of Clay to Structures with Different Materials. *Geofluids* **2021**, *2021*, 3794889. [[CrossRef](#)]

19. Lee, H.; Kim Kim, D.Y.; Shin, D.; Oh, J.; Hangseok, C. Effect of foam conditioning on performance of EPB shield tunnelling through laboratory excavation test. *Transp. Geotech.* **2022**, *32*, 100692. [[CrossRef](#)]
20. Gong, Q.; Wu, F.; Wang, D.; Qiu, H.; Yin, L. Development and Application of Cutterhead Working Status Monitoring System for Shield TBM Tunnelling. *Rock Mech. Rock Eng.* **2021**, *54*, 1731–1753. [[CrossRef](#)]
21. Yang, Y.; Li, X.; Jin, D.; Su, W.; Mao, J. Transient temperature field model for a cutterhead during slurry shield tunneling. *Tunn. Undergr. Space Technol.* **2021**, *117*, 104128. [[CrossRef](#)]
22. Wang, F.; Luo, F.; Huang, Y.; Zhu, L.; Hu, H. Thermal analysis and air temperature prediction in TBM construction tunnels. *Appl. Therm. Eng.* **2019**, *158*, 113822. [[CrossRef](#)]
23. Sahinoglu, U.K.; Ozer, U. The prediction of cutter wear from temperature measurements on TBM discs and cutting face. *Arab. J. Geosci.* **2020**, *13*, 207. [[CrossRef](#)]
24. Shi, H.; Yang, H.; Gong, G.; Wang, L. Determination of the cutterhead torque for EPB shield tunneling machine. *Autom. Constr.* **2011**, *20*, 1087–1095. [[CrossRef](#)]
25. Meschke, G.; Nagel, F.; Stascheit, J. Computational Simulation of Mechanized Tunneling as Part of an Integrated Decision Support Platform. *Int. J. Geomech.* **2011**, *11*, 519–528. [[CrossRef](#)]
26. Budach, C.; Thewes, M. Application ranges of EPB shields in coarse ground based on laboratory research. *Tunn. Undergr. Space Technol.* **2015**, *50*, 296–304. [[CrossRef](#)]
27. Kim, T.H.; Kim, B.K.; Lee, K.H.; Lee, I.M. Soil Conditioning of Weathered Granite Soil used for EPB Shield TBM: A Laboratory Scale Study. *KSCE J. Civ. Eng.* **2019**, *23*, 1829–1838. [[CrossRef](#)]
28. Peila, D.; Oggeri, C.; Borio, L. Using the slump test to assess the behavior of conditioned soil for EPB tunneling. *Environ. Eng. Geosci.* **2009**, *15*, 167–174. [[CrossRef](#)]
29. Yuan, Y.; Chen, W.; Zhao, J. The Effect of Organic and Inorganic Modifiers on the Physical Properties of Granite Residual Soil. *Adv. Mater. Sci. Eng.* **2022**, *2022*, 9542258. [[CrossRef](#)]
30. Wan, Z.; Li, S.; Yuan, C.; Zhao, S. Soil Conditioning for EPB Shield Tunneling in Silty Clay and Weathered Mudstone. *Int. J. Geomech.* **2021**, *21*, 6021020. [[CrossRef](#)]
31. Xiao, X.; Xia, Y.; Mao, X.; Wang, Y.; Fang, Z.; Wang, F.; Zhao, H. Effect of the nozzle structure of the large-diameter slurry shield cutterhead on the scouring characteristics. *J. Braz. Soc. Mech. Sci. Eng.* **2020**, *42*, 157. [[CrossRef](#)]
32. Thewes, M.; Hollmann, F.; Zhao, J. Assessment of clay soils and clay-rich rock for clogging of TBMs. *Tunn. Undergr. Space Technol.* **2016**, *57*, 122–128. [[CrossRef](#)]
33. Feng, H.; Chen, K.; Wang, Z. Research on High-efficiency Rock Fragmentation of TBM Cutter-head. In *Applied Mechanics and Materials*; Trans Tech Publications Ltd.: Bäch, Switzerland, 2013; pp. 1398–1403. [[CrossRef](#)]
34. Lu, X.; Wei, X. Experimental Study on Ionic Soil Stabilizer Reinforcing Red Clay. In *Advanced Materials Research*; Trans Tech Publications Ltd.: Bäch, Switzerland, 2011; p. 1736. [[CrossRef](#)]
35. Vasilopanagos, C.; Carteret, C.; Hillier, S.; Neumann, A.; Brooksbank, H.; Greenwell, H. Effect of Structural Fe Reduction on Water Sorption by Swelling and Non-Swelling Clay Minerals. *Minerals* **2022**, *12*, 453. [[CrossRef](#)]
36. Yuan, B.; Chen, M.; Chen, W. Effect of Pile-Soil Relative Stiffness on Deformation Characteristics of the Laterally Loaded Pile. *Adv. Mater. Sci. Eng.* **2022**, *2022*, 4913887. [[CrossRef](#)]
37. Wapshott-Stehli, H.L.; Grunden, A.M. In situ H₂O₂ generation methods in the context of enzyme biocatalysis. *Enzym. Microb. Technol.* **2021**, *145*, 109744. [[CrossRef](#)]